Improving System Stability Using Variable Switching Frequency with Boost-Type Power Factor Correction Converters

Dr. Prakash A. Kharade[1*], Zunzarrao V. Thorat[2], Dr. Shankar M. Patil[3], Dr. Kushal D. Badgujar[4]

[1*]Associate Professor, Bharati Vidyapeeth College of Engineering, Navi Mumbai, Maharashtra 400614, Email: kharadepa@yahoo.co.in

[2]Asst. Professor, Bharati Vidyapeeth College of Engineering, Navi Mumbai, Maharashtra 400614, Email:zunzar_thorat@rediffmail.com

[3]Associate Professor, Bharati Vidyapeeth College of Engineering, Navi Mumbai, Maharashtra 400614, Email: smpatil2k@gmail.com

[4]Asst. Professor, Bharati Vidyapeeth College of Engineering, Navi Mumbai, Maharashtra 400614, Email: drkushal.badgujar@bvcoenm.edu.in

Abstract: The power factor correction (PFC) in switching power supplies and a hybrid control technique called segmented PI repetitive sliding mode (PIR-SMC) highlight a control for DC and AC voltage regulation. Challenges in boost-type PFC converters include maintaining stability, reducing harmonic currents, and optimizing control loops. This method ensures the best dynamic behaviour, reduces overvoltage, and quickly responds to changes in voltage or load current. A proportional-integral (PI) control is used to minimize steady-state errors, and a switching surface function is constructed using the average dwell time methodology and positive diagonally dominating Lyapunov functional method. Adaptive Hysteresis Band (AHB) ensures steady switching frequency and lower distortion. The Floquet theory is employed to analyse stability, and the Grasshopper Algorithm (GA) optimizes control parameters. The study demonstrates the efficiency of the PIR-SMC approach through simulation and experimentation on a 630W universal-line PFC prototype, showcasing the fundamental frequency (50 Hz) at 19.78% and the overall THD at 1.81%. Future scope for improvement includes exploring advanced control strategies, integrating adaptive techniques, and employing advanced filtering methods to enhance system stability.

Keywords: Proportional-Integral**,** Buck and Boost, Floquet Theory, Power Factor, Grasshopper Algorithm, Converter Efficiency.

1. INTRODUCTION

Present-day applications for DC/DC converters include electric vehicles, power factor correction (PFC) circuits, dynamic filters, DC/DC regulated power supply, suitable ages, etc. When a conversion between two DC voltage levels is required, DC/DC converters are used. A buck-boost converter, also known as an exchanged mode power supply, combines the standards of a boost converter and a buck converter into a single circuit [1-2-3]. Interleaved converters have been increasingly popular in recent years and offer many benefits, including increased efficiency, high load power, and reduced voltage and current ripples. A significant problem is the DC/DC converter efficiency. For the converters' careful switching operation, various control approaches and converter topologies are thus suggested to achieve the lowest switching losses, highest efficiency, and most effective [4-5]. Rectifiers or AC/DC converters play a key role in powering DC loads from AC sources. Most DC loads used for industrial or domestic purposes include rectifiers to obtain the necessary DC voltage from the grid. A capacitor and a diode or thyristor bridge are typically used in rectifiers to create an electrical output that is roughly constant and can fulfil the power demand [6-7-8]. As switching power supplies frequently consumes large currents in a short time, distorted current outputs ensue; PFCs are

designed to enhance the power quality of the supplies. Because it is simple to operate, has less switching stress than other configurations, and incorporates an input side inductor filter that rejects unavoidable discontinuities in the input current waveform, a boost converter provides the simplest alternative for 1-phase PFC [9-10]. The bidirectional 1-phase buck-boost rectifier for PFC is introduced in [11-12]. The buck PFC uses has been made possible by the PFC converter's effectiveness at the buck converter's low voltage region, but the main drawback is the existence of a dead angle, where the power factor is degraded. As a result, actions need to be taken to reduce the dead angle [13-14].

The popular topology for PFC rectifiers utilizes a boost converter along with a control system. Nevertheless, controllers are created using linearized modelling of the converters for a particular operating point; the needed entire system's stability and the dynamic performance for other operating points are still not assured [15-16]. When there are several power converters in a system, the overall current may display zero-crossing distortion as large, repeated damped oscillations. The power system's frequency is coordinated with these oscillations and a 1-phase AC/DC converter input current when equipped with a PFC controller [17-18]. The 3-phase boost PFC rectifier system is presented with a PI controller in [19-20] to model and control the PFC system. A simplified small-signal model with segmented control action for control transfer functions has been proposed to overcome combining traditional PI control cons with complicated control transfer functions. A PID controller that uses proportional, derivative, derivative filter coefficient constants, and integral to control PFC is optimized using a particle swarm optimization technique [21-22]. For power quality enhancement, the adaptive control algorithm of the Robust Shrine Affine Projection Sign is used [23-24]. It is possible to employ a 5-level Cascaded H-Bridge multilevel inverter to get around the drawbacks of traditional 2-level inverters. By employing PI controllers, the capacitor's DC link has been kept at a reference value without the use of intricate balancing circuits.

The stability analysis (SA) is conducted in a phase-shifted full-bridge (PSFB) zero-voltage switch circuit [25-26]. The fractional-order stability analysis of the estimated dynamic model's tuning guidelines and the error feedback controller's gains are retrieved using the linear matrix inequality (LMI) technique and fuzzy logic compensator [27-28]. The power systems' small-signal stability has emerged as one of the major issues with the development of energy sources. As a result, a power system with a wind farm and a PV module combined must have small-signal stability. The voltage drop at various nodes supports the correctness of the idea and demonstrates how quickly a power system with solar and wind-powered renewable energy sources may restore the system to its rated frequency while also boosting the durability of every unit [29-30]. The stability of a hybrid power system's frequency examined, a Fractional Order PID controller, combined with Matignon's theorem, is utilized to enhance the control and analysis process [31]. This study contributes by introducing a variable switching frequency approach to enhance system stability in boost-type power factor correction converters. By dynamically adjusting the switching frequency, the method effectively mitigates stability issues and reduces harmonic distortion. This approach offers improved performance and reliability over traditional fixed-frequency methods, making it a valuable advancement in PFC converter design. The research objective of improving system stability using variable switching frequency with boost-type power factor correction converters is to enhance the stability of power systems by employing variable switching frequency techniques in conjunction with boost-type power factor correction (PFC) converters. The focus is on optimizing system performance by adjusting the switching frequency of the converters to address stability issues, improve efficiency, and reduce the potential for instability caused by fixed switching frequencies. This approach aims to achieve better control over power quality, reduce harmonic distortion, and enhance the overall reliability and performance of the power conversion process. The challenge of improving system stability in Boost-type Power Factor Correction

(PFC) converters using variable switching frequency has been widely discussed, but most existing research focuses on specific conditions like steady-state performance or limited load scenarios. There is a lack of studies that comprehensively address the dynamic adjustment of switching frequency to maintain stability under varying input and load conditions. This gap leads to suboptimal performance in terms of transient response, ripple current, electromagnetic interference (EMI), and thermal management, highlighting the need for an innovative approach that ensures consistent stability across diverse operational environments. The remaining sections are arranged as follows: The literature review was as stated in Section 2, the problem definition and motivation in Section 3, the proposed technique was labelled in Section 4, the results were discussed in Section 5, and the paper's conclusion was described in Section 6.

2. REVIEW OF LITERATURE

Regulated constant power loads have a progressively negative input impedance that may cause the linked system to become unstable. An unstable dynamic relationship between the load and source impedance might occur with AC and PFC constant power loads. The rectifying contact dynamics are nonlinear and thus elude traditional stability and impedance analysis. Understanding and characterizing the crucial dynamic interplay between AC sources and AC PFC converters has been the focus of numerous attempts. A realistic AC PFC converter model with a programmable controller that can govern source-load interactions was provided by Gutierrez *et al* [32]. For assessing AC sources and PFC loads, a specific envelope impedance approach was created. The illustration demonstrates an instability resulting from a hardware incompatibility issue between the load and source envelope impedance, along with a fluctuating power load that changes its bandwidth. This instability can be rectified by addressing the compatibility problem and managing the power load effectively, ensuring stability in the system.

A nonlinear load with a 1-phase half-bridge interleaved buck-shunt active power filter (HBIB-SAPF) was first controlled nonlinearly by Echalih *et al* [33]. The DC capacitor voltage of the HBIB converter was closely controlled while reactive and harmonic current consumption by the nonlinear load were compensated. To maintain a unity power factor, the inner loop controls the switching components so that its reference is followed by the active filter current. Employing a pre-filter and PI controller, the outer loop was responsible for controlling the DC capacitor voltage to the appropriate value. The closed-loop system stability analysis was formally carried out by applying the averaging theory. Gopi *et al* [34] investigated the PID co-efficient tuning using the Tree-Seed Algorithm. In a DC motor drive using a PID controller, the disk-based margins were presented to assess the feedback loop for dependable stability against gain and phase instability. According to the analysis, the suggested strategy has high reliability and a wide range of stability margins for the feedback loop uncertainty.

To achieve the application of PFC and voltage regulation as well as increased resilience, performance and efficiency features of the converter, Sepperumal *et al* [35] suggested a controller called optimized fractional-order PI (FOPI) for a DC-DC SEPIC converter. For the inner current and outer voltage control loops of the DC-DC SEPIC model, an atom search optimization was suggested. Based on the simulation results, the suggested technique offers a more dominating dynamic response, increased power factor, and efficiency. However, the SEPIC converter has a complex control loop. Therefore, Ortiz-Castrillón *et al* [36] proposed a Semi-Bridgeless Boost Converter for PFC and DC bus regulation. System stability was improved by including an AC error term integral. The Adaptive Hysteresis Band (AHB) is employed to maintain a consistent switching frequency and minimize distortion at zero crossings, while simultaneously managing AC voltage and DC. To further enhance the control method, a Hybrid PI-Sliding Mode Control approach is utilized. The study investigates the proposed system's robustness during start-up and under significant disturbances.

The Bus-current controlled converter (BCCC) and Bus-voltage-controlled converter (BVCC) were introduced by Ruan *et al* [37] to create multi-converter systems. It is possible to include a second harmonic current compensator (SHCC) to replace the undesirable electrolytic capacitor. The impedance-based stability criterion was used to investigate the system stability. To ensure system stability, in BVCC tenders that employed the AC-DC stage, a virtual resistor was created and implemented via the SHCC control scheme. An LCL coupling circuit-based shunt active power filter with closed-loop control and predictive current controller for SHCC was presented by Bieleck *et al* [38]. The control system's stability analysis with the additional exterior supply current control loops and current predictive control was therefore examined. The stability analysis that was undertaken includes an assessment of the system's stability concerning the precision with which the coupling circuit parameter was identified. The two-stage energy conversion mechanism issues are resolved for large industrial driving applications of direct matrix converter (DMC). The operation of multiphase drives by DMC raises serious concerns because of a shortage of technological improvement. So, for a 5-phase induction motor controlled by a three-to-five-phase DMC, Muduli *et al* [39] provide a direct torque control approach based on space vector PWM. A control strategy for an automobile DC/DC converter was presented by Korte *et al* [40] that lower the EMI produced by predicting switching distortion during operation. The multi-step model-predictive control technique selects the next switching state that maximizes the output spectrum based on predetermined criteria. A single unified control law was used to regulate both the switching rate and the voltage ripple. However, applying nonlinear load results in a low power factor, which has an impact on voltage regulation, conductor losses, price, and machine rating. Shah *et al* [41] presented the main cause of harmonics, which raises THD in the distribution system and lowers power factor, is nonlinear loads. Large-value capacitors are typically employed in full-bridge diode rectifiers to produce cleaner DC output. As a result, the supply side was introduced to current harmonics by using big-value capacitors. Venkataramana *et al* [42] Developed a scalable key organization plan for Wireless Sensor Networks (WSN) using the unital style concept while focusing on performance evaluation and energy efficiency in security trade-offs. The Result proposed energy analysis module for QoP-ML aids in evaluating the impact of different security levels on WSN protocols' energy consumption, addressing challenges in WSN applications. Liu *et al* [43] proposed a synchronous alteration control method for AC/DC converters using a response surface algorithm to enhance stability and anti-interference capabilities. The method involves designing a high-speed, low-power comparator to compare input and output signals. Test results demonstrate that the converter's output waveform is stable and regular with good phase-shifting characteristics. Djebbri *et al* [44] focused on controlling electrical energy transfers in multi-source renewable energy systems, specifically examining a system with photovoltaic and lead-acid battery bank sources, a full-bridge isolated buck DC/DC power converter, and a load. The results in a system with two cascaded loops: an inner loop for current control and an outer loop for output voltage control using PI and PID controllers. Badal *et al* [45] addressed the significance of damping torque control in synchronous machines within power systems, a high-performance controller is proposed, integrating the Linear Quadratic Gaussian (LQG) and integral controller. The findings show the level of uncertainty of the proposed controller with the Linear Quadratic Regulator (LQR), LQG, and Linear-Quadratic-Integral (LQI) controllers to validate its effectiveness. Ahmad *et al* [46] proposed angular velocity tracking of dc motors powered by dc/dc buck converters. The Global Simultaneous Perturbation Stochastic Approximation (GSPSA) method is employed to optimize the sigmoid-based PI parameters, ensuring fast tuning without relying on plant models. The approach has been successfully validated on a well-known buck converter-powered DC motor model, demonstrating improved tracking performance and duty cycle compared to existing methods. Cisneros *et al* [47] developed a linear time-varying PI controller

for trajectory tracking of bilinear systems with time-varying measurable disturbances, using a set of identified matrices {A, Bi} and ensuring global tracking.

Summarize Key Findings: Begin by briefly highlighting the main contributions and findings from the reviewed literature. Emphasize significant methods and results related to power converter stability, control techniques, and challenges.

Identify Common Themes and Gaps: Point out common themes across the studies and any gaps or limitations identified. This might include complexities in existing methods, limitations in practical applications, or areas where current approaches fall short.

Connect to Study Objectives: Clearly state how your study addresses these gaps or limitations. Explain how your approach using variable switching frequency with boost-type PFC converters offers a simpler, more effective solution.

Highlight Contributions: Mention how your research contributes to the field, such as improving stability, efficiency, or implementation practicality.

End with Implications: Conclude with a statement on the potential impact of your study and its relevance to future research or practical applications.

The literature review reveals a variety of methods for enhancing stability in power converters, including sliding mode control, optimization techniques, and advanced controller designs. Despite their effectiveness, these methods often involve complex implementations and practical limitations. This study proposes a novel approach utilizing variable switching frequency in boost-type power factor correction converters to address these challenges. By simplifying the control strategy and improving system stability and efficiency, this approach fills critical gaps identified in past research. The proposed method not only enhances system performance but also offers a more accessible and practical solution for real-world applications, paving the way for future advancements in power converter technology.

Despite advancements in power factor correction (PFC) and converter control strategies, existing methods often struggle with system instability under constant power loads and varying dynamic conditions. Many traditional controllers lack adaptability, and simulation-based solutions frequently face implementation challenges due to complexity and limited scalability. This research addresses these gaps by introducing an adaptive hybrid control approach combining Proportional-Integral-Repetitive Sliding Mode Control (PIR-SMC) and Adaptive Hysteresis Band (AHB). Validated through simulation and experimentation, the method ensures improved dynamic performance, reduced total harmonic distortion (1.81%), and enhanced stability. This work advances the field by offering a robust, scalable solution for modern PFC systems.

3. PROBLEM DEFINITION AND MOTIVATION

Single-phase switch-mode AC-DC power converters, particularly boost converters, are widely employed due to their efficiency and compact design. Despite their advantages, they introduce harmonic currents into the utility line, leading to low input power factors. Boost-based PFC (Power Factor Correction) rectifiers are popular in the literature for their cost-effectiveness, simplicity, and ease of analysis and control. Various DC/DC converter topologies can be utilized in PFC rectifiers, with boost converters being the most preferred. To develop an optimal control loop for power converters by focusing on small-signal stability modelling and appropriate stability criteria [48-52]. The exploration highlights designing a control loop that ensures efficient regulation of output voltage and inductor current reference in boost converters. By employing suitable stability criteria, to enhance the overall performance the method targets the reliability of single-phase switch-mode AC-DC power converters.

4. PROPOSED RESEARCH METHODOLOGY

Efficient transformation of alternating current (AC) into direct current (DC) while maintaining a high power factor and minimal total harmonic distortion, power factor correction (PFC) rectifiers play a vital role. The most common PFC rectifier architecture integrates a power stage, which comprises a Diode Bridge and a Boost converter, with a control system. However, there is a control challenge as the system's dynamic performance and stability across different operating conditions cannot be assured, as controllers are developed using linearized models of the converters for specific operational scenarios. The proposed work's flow diagram is represented in Figure 1.

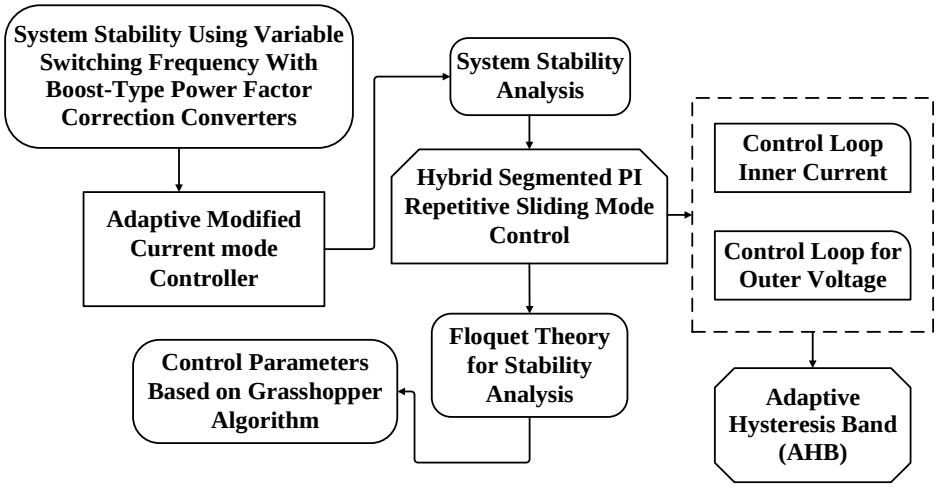

Figure 1: Flow Diagram of the Research Work

Figure 1 shows adaptive nonlinear control based on passivity is utilized to control boost converters used for PFC in applications for universal lines with uncertain loads. Based on the examination of the internal dynamics brought on by the use of the suggested control technique, it is investigated whether the closed-loop system is stable. An experimental 630-W universal-line PFC prototype is used to test the suggested PFC rectifier's performance. This research effort focuses on the boost rectifier's control with PFC when there is a variable load resistance. To achieve minimal line current distortion and increased dynamic performance, the regulation is done using an AMCMC. This control provides the optimum dynamic behaviour by eliminating DC overvoltage and quickly adapting to changes in DC voltage or DC load current. AHB is used to maintain a steady switching frequency and lessen distortion during zero crossings. Floquet theory is employed for analysing the closed-loop system's stability. To have more control loops it's important to make the control design more difficult. The Grasshopper Algorithm (GA) is used to optimise the control parameters, which can ultimately lessen the complexity of the control design.

4.1 Adaptive Modified Current Mode Controller (AMCMC)

During the erratic load resistance, the boost rectifier's control with PFC is addressed. To achieve minimal line current distortion and increased dynamic performance, the regulation is done using an AMCMC. All the desired characteristics of the current-mode controllers are present in the controller.

The hybrid-type boost converter's adaptive current-mode control law is provided in the following equation.

$$u = U - K_c\left[x_i - \hat{X}_i\left(\hat{\theta}\right)\right], \quad i = 1,2 \tag{1}$$

Where Equation (1) represents the adaptive current-mode control law for a hybrid-type boost converter. K_c is the adaptive controller's gain, U is determined by (2), and x_i is the

converter's inductor current, whose reference value $\hat{X}_i(\hat{\theta})$ is obtained using the load conductance estimator and $i = 1, 2$ represents two different inductor currents. The estimator $\hat{\theta}$ is created by applying the adaptive law provided by

$$U = \frac{V_d - E}{V_d + E} \tag{2}$$

Equation (2) determines the value of U represents the averaged equilibrium values of the state variables, the converter's input. V_d and output E is linked as.

$$\frac{d\hat{\theta}}{dt} = -\frac{2\beta m e_3}{1+\beta^2 e_3^2} \tag{3}$$

Equation (3) describes $\hat{\theta}$ is the estimated value of the load conductance. As the actual load changes, this estimate must adapt accordingly to maintain performance. $\frac{d\hat{\theta}}{dt}$ is the rate of change of the estimated conductance this tells how the estimate should be updated over time. β A positive tuning parameter that controls how aggressively the estimate is adjusted. A higher β leads to faster updates but may introduce noise or instability. m is the scaling factor that influences the magnitude of the adaptation. e_3 is the estimation error, typically the difference between actual and predicted values related to output or inductor current.

The following is the control law utilizing the input inductor current:

$$u = U - K_c[x_1 - \hat{X}_1] \tag{4}$$

Equation (4) is the control law using the input inductor current. It helps regulate the control signal u based on the difference between the actual input inductor current. x_1 and the estimated reference input current $\hat{X}_1$.

Where, $\hat{X}_1 = \frac{\hat{\theta} V_d^2}{E}$. $\hat{X}_1$ is x_1 estimated value, and $\hat{\theta}$ is determined using a new equation, which also involves the input voltage V_d using (5). For a better understanding of the adaptive current-mode controlled system Stability Analysis is counted. e_1 to e_4 represent the errors between the actual and estimated inductor currents and load conductance estimation error $\tilde{\theta}$.

In this equation, the ensuing mistakes are defined.

$$e_1 = \bar{x}_1 - X_1,\ e_2 = \bar{x}_2 - X_2,\ e_3 = \bar{x}_3 - X_3,\ e_4 = \bar{x}_4 - X_4,\ \tilde{\theta} = \hat{\theta} - \frac{1}{R} \tag{5}$$

Substituting (1) - (5) into the average state space model yields the error dynamics described by

$$\frac{d\tilde{\theta}}{dt} = -\frac{2\beta m e_3}{1+\beta^2 e_3^2} \tag{6}$$

Where,

$$u_{e1} = U - K_c\left(e_1 - \frac{\tilde{\theta} V_d^2}{E}\right) \tag{7}$$

The equation (7)'s equilibrium points can be obtained from the original control law (1) and involves the input inductor current estimation

$$e_{1\infty} = e_{2\infty} = e_{3\infty} = e_{4\infty} = \tilde{\theta}_\infty = 0 \tag{8}$$

Equation (8) shows the equilibrium points of the system when all errors ($e_{1\infty}$, $e_{2\infty}$, $e_{3\infty}$, $e_{4\infty}$) and the load conductance estimation error $\tilde{\theta}_\infty$ are zero. The following linearized system results from linearizing (10) near the stability point.

$$\dot{z} = M_{in^z} \tag{9}$$

The controller gains required to maintain system stability for the non-linear adaptive controller developed utilising the input inductor current are rather constrained.

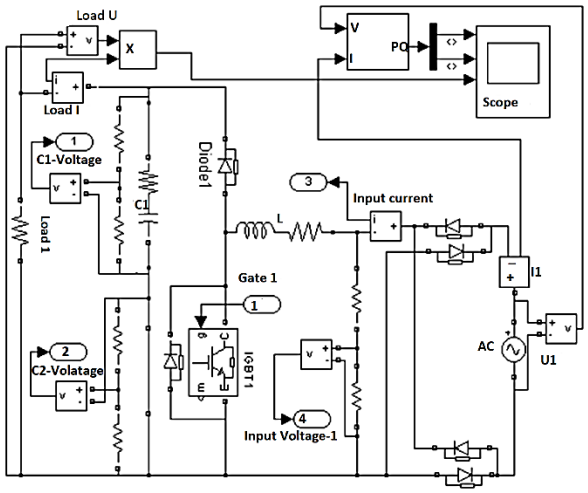

Figure 2: MATLAB Model of Power of Boost PFC Converter

Figure 2 showcases a MATLAB model representing the power of a Boost Power Factor Correction (PFC) Converter. This model serves as a visual representation of the theoretical framework used to simulate and analyse the behaviour of the Boost PFC Converter within the MATLAB environment. Typically, such models include mathematical equations, circuit diagrams, and simulation results to illustrate the dynamic behaviour and performance characteristics of the converter under various operating conditions. Researchers and engineers utilize these models to design, optimize, and validate the performance of Boost PFC Converters, facilitating advancements in power electronics and energy conversion systems.

4.2 System Stability Analysis

Various techniques, such as the eigenvalue analysis using the system's state-space model in the time domain and the impedance-based analysis based on the TFs components of the frequency domain, have frequently been employed to test the system-level stability. However, from a control perspective, the Nyquist stability criterion (NSC) and loop gain analysis in the frequency domain are two straightforward and frequently used graphical approaches used to examine the stability of PI and repeated control-based systems. For a very long time, three-phase power electronic topologies, whose control action has been primarily based on PI and repeated control methods, have successfully implemented such stability conditions. The methodologies have demonstrated improved performance for the system with implemented digital control. The findings in the next sections provide an explanation of the stability performance based on NSC and loop gain utilizing a Bode plot for both loops.

4.2.1 Sliding Mode Control

The equilibrium is maintained between a hybrid microgrid system and its AC load, an advanced control and power management system is employed. This system, which utilizes sliding mode control for both DC and AC loads, offers the flexibility and efficiency needed to regulate power flow through the converters of all components. By managing DC voltage and AC, it allows for effective power distribution. The reference current is determined by the power balance, while the control signal is derived from an adaptive hysteresis band. The benefits and drawbacks of the hybrid PI-SMC and SMC controllers are assessed using the proposed sliding surface.

Table 1: PI-SMC vs. PI Controller Performance Comparison

Aspect	PI-SMC	PI Controller
Disturbance	Superior	Moderate
Non-linearities	Can handle non-linear systems better	May struggle with significant non-linearities
Fast Settling Time	Achieves faster settling time in many cases	Settling time can be slower
Parameter Tuning	More complex parameter tuning process	Simpler parameter tuning
Computational Cost	Higher computational complexity	Lower computational complexity

Table 1 shows the performance advantage of PI-SMC can vary depending on the specific system dynamics. A well-tuned PI controller might be sufficient. The more complex parameter tuning and potential for chattering in PI-SMC can make it more challenging to implement compared to the simpler PI controller. PI-SMC offers superior performance in many aspects compared to a PI controller, but it comes with increased complexity. The choice between them depends on the specific application requirements and resource constraints.

4.2.2 Segmented PI-Repetitive Control

The inner current loop 15 and voltage loop 17, which have similar transfer functions, significantly impact the system's steady-state characteristics, such as load voltage. V_{dc} and load resistance R_L. However, using a fixed set of PI control parameters or parallel PI-repetitive control parameters 21 and 22 may not be effective under various load conditions. This issue addressed, variable PI-repetitive control settings are employed to enable the system to adapt to different working situations. Although numerous control parameters can be designed for various load sizes, only a limited number can be considered in practice. To manage these control actions, a segmented PI-repetitive control approach is proposed, dividing the system into three portions based on rated load percentage, with specific control settings for each area. Hysteresis is used to switch the overlap between segments, preventing oscillations and abrupt changes in controller parameters, and ensuring system stability and quick response times.

The Segmented PI control algorithm consists of multiple PI controllers operating in different segments or regions of the control space. Each segment has its own PI controller gains (Kp and Ki) to adapt to the specific system dynamics within that region. The overall control strategy divides the system's operation range into several segments, and for each segment, a separate PI controller is designed. The equations for a typical Segmented PI controller in its i-th segment can be represented as follows.

For Control Error,

$$e(t) = r(t) - y(t) \tag{10}$$

For Proportional Terms,

$$u_{p(t)} = K_{(p)i} * e(t) \tag{11}$$

For Integral Terms,

$$u_{i(t)} = K_{(i)i} * \int e(t)\, dt \tag{12}$$

For Segmented PI Output,

$$u(t) = U_{(t)i} + u_{i(t)} \tag{13}$$

Where,

$e(t)$is the control error at time t, which is the difference between the reference input (r(t)) and the system output $y(t)$.

$K_{(p)i}$ and $K_{(i)i}$ are the proportional and integral gains, respectively, for the i-th segment.

These gains are chosen based on the specific dynamics of the system within that segment.

$u_{p(t)}$) output of proportional controller at time t.

$u_{i(t)}$ the output of the integral controller at time t.

$u(t)$ is the overall output of the Segmented PI controller at time t, which is the sum of the proportional and integral.

The number of segments and the boundaries between them depend on the specific system being controlled and the desired performance. The gains for each segment are typically determined through experimental tuning or optimization techniques like the Grasshopper Algorithm (GA) to achieve the best control performance for the given application.

Control Loop for Outer Voltage

By adjusting the control current I_{DC} flowing to the capacitor CDC to its reference current I_{DC_Ref}, one can control a DC-link voltage V_{DC} to its desired voltage V_{DC_Ref}. The PI controller is responsible for regulating the voltage in the outer loop frequency domain for its implementation:

$$I_{DC_{Ref}}(P) = C_{PI}(P) \cdot \left(V_{DC\_Ref} - V_{DC}(P)\right) \tag{14}$$

Equation (14) represents to control of the DC-link voltage V_{DC} to its desired value V_{DC_Ref} can be translated into the time domain using the Inverse Laplace Transform as follows:

$$I_{DC_{Ref}} = K_P \cdot \left(V_{DC_{Ref}} - V_{DC}\right) + K_i \int \left(V_{DC_{Ref}} - V_{DC}\right) dt \tag{15}$$

Equation (15) is the time-domain version of equation (10) after applying the Inverse Laplace Transform. It shows the relationship between the control current. $I_{DC_{Ref}}$ and the voltage difference $\left(V_{DC_{Ref}} - V_{DC}\right)$. Where, K_P and K_P are the (PI) controller's parameters. By using Kirchhoff's current law, it obtained as follows:

$$I_{DC} = I_{PS1\_DC} + I_{PS2\_DC} + I_{PS3\_DC} + I_{B\_DC} - I_{Load} \tag{16}$$

Equation (16) is Kirchhoff's current law applied to the circuit. It states that the total current I_{DC} in the circuit is the sum of the currents from the power system boost converters, the battery bidirectional converter, and the load current, $I_{PS1\_DC}, I_{PS2\_DC}, I_{PS3\_DC}$ and I_{B_DC} are, respectively, the output currents of the power system boost converters and the current of the battery bidirectional converter. The output current can be determined from the input current by applying the power conservation equation. $P_{in} = P_{out}$. The loss of power is not considered. Equation (13) is expressed as follows:

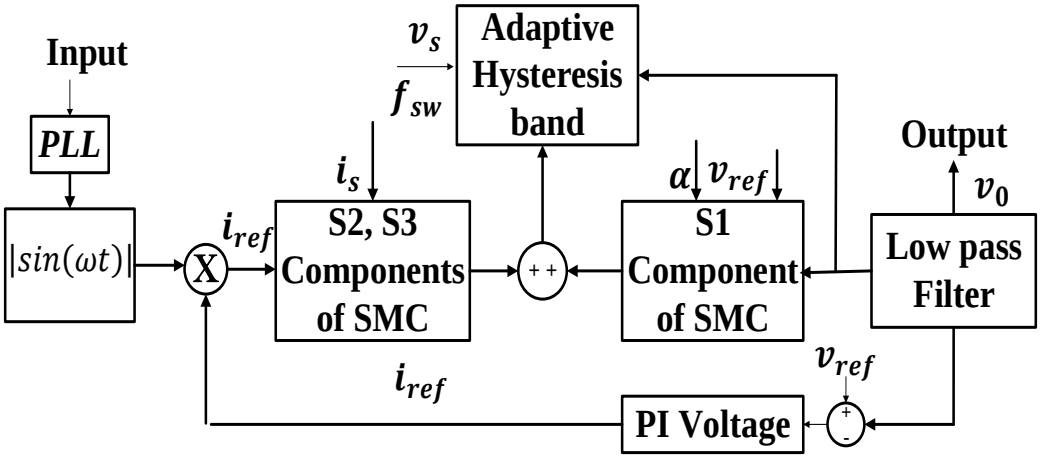

Figure 3: Block Diagram of the Outer Voltage Control Loop Using PI-SMC Controller

$$I_{DC} = \frac{1}{V_{DC}} \cdot (I_{PS1} \cdot V_{PS1} + I_{PS2} \cdot V_{PS2} + I_{PS3} \cdot V_{PS3} + I_B \cdot V_B - I_{Load} \cdot V_{DC}) \quad (17)$$

Equation (17) is a modified version of equation (12) that considers the DC-link voltage. V_{DC} and the voltage levels of the power system boost converters (V_{PS1}, V_{PS2}, V_{PS3}) and the battery V_B.Where, I_{DC} is merely reference-regulated to its current using IB from the battery. Hence, rewrite equation (13) as follows:

$$I_{DC\_Ref} = \frac{1}{V_B} \cdot \left(I_{DC\_Ref} \cdot V_{DC} + I_{Load} \cdot V_{DC} - I_{PS1} \cdot V_{PS1} + I_{PS2} \cdot V_{PS2} + I_{PS3} \cdot V_{PS3}\right) \quad (18)$$

Equation (18) relates the reference current for the DC-link I_{DC_Ref} to the battery current V_B, the DC-link voltage V_{DC}, besides $the\ load\ current\ I_{Load}$.

A PI-SMC controller is a powerful control strategy that integrates the Proportional-Integral (PI) controller and the Sliding Mode Control (SMC) block in Figure 3. This combination offers enhanced performance by leveraging the strengths of both components. The PI controller adjusts the system output based on the current error (the difference between the desired and actual output) and the accumulated error over time, providing a gradual and stable response. On the other hand, the SMC block ensures quick convergence to the desired state and maintains it by introducing a switching function that drives the system error towards a specific sliding surface, which represents a zero-error line.

Table 2: Controller Parameter Comparison Table

Controller Type	Proportional Gain (Kp)	Integral Gain (Ki)	Super-Twisting Gain (λ)
PI	0.5	0.1	-
PI-SMC	0.4	0.08	0.5
PI-SMC and PI Combined	0.45	0.09	0.5

In the presented table 2, three different types of controllers are outlined: Proportional-Integral (PI), Proportional-Integral-Sliding Mode Controller (PI-SMC), and a combined approach of PI-SMC and PI. Each controller is characterized by specific values of Proportional Gain (Kp), Integral Gain (Ki), and Super-Twisting Gain (λ). The PI controller exhibits a proportional gain of 0.5 and an integral gain of 0.1, while the PI-SMC controller adjusts these parameters slightly with a proportional gain of 0.4 and an integral gain of 0.08, accompanied by a Super-Twisting Gain of 0.5. Interestingly, the combined approach integrates elements from both controllers, with proportional and integral gains set at 0.45 and 0.09, respectively, while maintaining the Super-Twisting Gain at 0.5. This comparison elucidates the variations in control strategies and parameter tuning employed to optimize system performance, providing insights for further analysis and experimentation in controller design.

Control Loop Inner Current

To quickly stabilise the battery current around the target value attained by the outer voltage loop, a Direct Sliding Mode Control (DSMC) is used. This choice is additionally supported by the DSMC's resistance to changes in system parameters. The controller that is the subject of the investigation makes the following claim.

Proposition 1. The equation given helps in selecting the appropriate switching function for a specific purpose.

$$s = I_{B\_ref} - I_B \quad (19)$$

Equation (19) defines the sliding function s for the Direct Sliding Mode Control (DSMC) in the inner current control loop. It helps maintain the battery's current. I_B around its reference value I_{B_ref}.For the boost mode to function:

$$u_{cmd\_5} = \frac{1}{2} \cdot \left(1 + sign(s)\right) \tag{20}$$

Equation (20) determines the control command u_{cmd_5} for the DSMC sliding-based function (s). It ensures battery current reaches its reference value quickly.

Equations (19) and (20) provide a control mode for sliding where the battery current reaches the goal value in a finite amount of time. The DC-link voltage also receives its reference value.

Having the sliding surface with $s = 0$ is preferred for a brief time, as it provides a suitable condition. By giving a live picture of the boost mode battery current:

$$\frac{di_B}{dt} = \frac{1}{L_B}\left(\left(u_{cmd\_5} - 1\right)V_{DC} + V_B\right) \tag{21}$$

Equation (21), describes the rate of change of the battery current $\frac{di_B}{dt}$ based on the control command u_{cmd_5}, the DC-link voltage V_{DC}, and the battery voltage V_B. The fact that $u_{cmd\_5} = 0$ when $s < 0$.

$$s\dot{s} = -\frac{1}{L_B}\underbrace{\left(I_{B_{Ref}} - I_B\right)}_{<0} \cdot \underbrace{\left(-V_{DC} + V_B\right)}_{<0} \Rightarrow \dot{V} < 0 \tag{22}$$

When $s > 0$, $u_{cmd\_5} = 1$ and

$$s\dot{s} = -\frac{1}{L_B}\underbrace{\left(I_{B_{Ref}} - I_B\right)}_{>0} \cdot \underbrace{\left(V_B\right)}_{>0} \Rightarrow \dot{V} < 0 \tag{23}$$

Equations (22) and (23) explain the sliding surface (s = 0) is attractive for a limited time when the system is in different modes. The sliding surface at $s = 0$ is alluring for a limited period. Based on the given equations, the battery current will eventually reach its target value, $I_{B_{Ref}}$, in a limited duration. This time depends on the initial situation and occurs in both modes. While the mode is active, just one command may be sent. The value of the other command is 0. Regions close to zero crossings that correspond to unstable points cannot, therefore, be regulated for the whole operational range. This criterion is not satisfied in a strict sense according to sliding mode theory. Practically speaking, the system becomes unstable in a short amount of time, and this is essentially why AC deforms at zero crossovers. Zero-crossing deformation can also happen when using different control strategies, not just in the context of the idea of sliding modes.

To improve the study on power factor correction (PFC) using the segmented PI repetitive sliding mode control (PIR-SMC) approach, it would indeed be beneficial to specify and analyze the system's performance under different load conditions. This would provide a more comprehensive understanding of how the control technique handles varying operational scenarios. Here's how you could address this:

Improving System Stability: System stability refers to the ability of a system to return to and maintain a desired operating point after experiencing a disturbance, without oscillating or diverging, which is essential for ensuring predictable and reliable performance in dynamic systems. The PIR SMC method enhances stability by leveraging three key components: Sliding Mode, which ensures the system remains on a predefined "sliding surface" despite external disturbances or nonlinearities; Resonant Control, which effectively rejects periodic or oscillatory disturbances, thus preventing resonance issues that could destabilize the system over time; and Integral Action, which eliminates steady-state error, ensuring the system converges to and maintains the desired state even in the presence of continuous disturbances.

Optimizing Control Loops: The PIR SMC method optimizes control loops by improving the system's response to changes in inputs or disturbances. It enhances response time by effectively rejecting disturbances and maintaining stability, allowing the system to react

quickly and accurately while minimizing delays and overshoot. The inclusion of PI and resonant terms improves accuracy, ensuring the system reaches and maintains the desired state with minimal error. Additionally, the sliding mode action helps in minimizing oscillations and overshoot, preventing excessive fluctuations, thereby enhancing overall control performance and efficiency.

Application of PIR SMC: The PIR SMC approach is highly effective in systems that require robustness, disturbance rejection, and stable control. It can be applied in power electronics, such as boost, buck, and power factor correction (PFC) converters, where periodic disturbances like harmonics can impact system performance. In motor control systems, PIR SMC can handle load variations and other periodic disturbances, ensuring precise operation. Robotics also benefits from this approach, as it enables precise control in the presence of dynamic loads or external forces. Furthermore, renewable energy systems, including wind and solar power generation, can use PIR SMC to maintain stability and efficiency amid fluctuating environmental conditions.

Adaptive Hysteresis Band (AHB)

According to Mejia-Ruiz, the AHB is created using the existing ripple geometry. It has two purposes: (1) reducing. THD_i by smoothing the present zero crossing; and (2) fixative frequency by modifying the switching time by the SBBC operation point. Equation (20) offers the AHB function of v_0, v_s, L and f_{sw}, while its execution is portrayed in Figure 2.

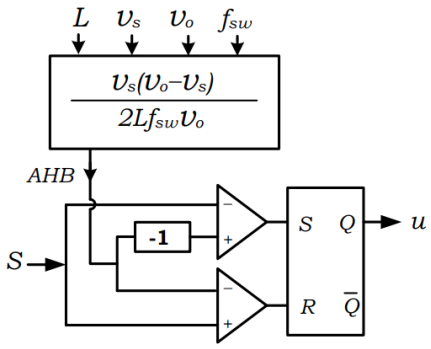

Figure 4: Adaptive Hysteresis Band Modulator

Figure 4 illustrates an Adaptive Hysteresis Band Modulator, it consists of a core component for calculating the modulation index based on input voltages (Vs and Vo) and switching frequency (fsw). This output is fed into a hysteresis comparator (AHB) which generates control signals (S and R) for switching elements (S and Q) based on the calculated modulation index. This modulator is designed to dynamically adjust the hysteresis band, enhancing control performance and potentially improving system efficiency and stability.

The sliding surface is contrasted with the AHB calculated at each point. The AC response of sliding mode control is instantaneous since PWM signals are not necessary for the AHB to operate across power switches.

$$AHB = \frac{v_s(v_0-v_s)}{2Lf_{sw}v_0} \tag{24}$$

By initiating, the behaviour of the AC error is assessed. After a few substantial transient oscillations in S2, the magnitude of oscillations is drastically reduced and is only perceptible at the initial zero crossings. S2 enters the convergence zone while oscillating in the AHB close to the equilibrium point. The primary role of S2 is to correctly follow the AC reference following load requirements, allowing for the avoidance of non-minimum phase behaviour. In

each cycle of the electric grid, the behaviour of S3 is reset during startup, making the accumulated error zero. Initially, S3 starts at zero, quickly drops to around -1.2 for the first peak, and then increases again to reach a stable zone close to S3 = 0. This provides strength against sudden changes, especially during startup, and helps reduce oscillations before reaching a steady state. The stabilization of DC voltage and AC during the startup of SBBC, along with the convergence of their errors (including integral) to zero, demonstrates the stability of the proposed sliding surface beyond the operating range.

Defining Load Conditions

Extreme Load Conditions: Identify scenarios where the load might be at its maximum or minimum limits. This could include cases of sudden load surges, drastic changes in load resistance, or high power demands. Testing under extreme conditions helps assess the robustness and responsiveness of the control strategy.

Normal Load Conditions: Specify typical operating conditions under which the system is expected to function under standard, everyday use. This helps establish baseline performance metrics and ensures the system operates efficiently under usual circumstances.

Experimental Setup

In the experimental setup, a Boost-Type Power Factor Correction (PFC) converter was employed, utilizing key power electronics components such as MOSFETs for switching, fast recovery diodes, inductors for energy storage, and high-quality capacitors for filtering purposes. The control system was managed by a microcontroller, specifically designed to implement variable switching frequency strategies, ensuring precise control of the converter's operation. The circuit design was carefully laid out with all components interconnected to optimize performance. Connections were meticulously arranged, with the PCB layout reflecting the need to minimize parasitic inductance and capacitance, thereby reducing electromagnetic interference. Key interactions between the MOSFETs, diodes, and passive components were carefully considered to ensure stability and efficiency. The power source for the experiments was derived from a standard AC mains voltage, carefully regulated to provide consistent input to the PFC converter. Various load conditions were applied during testing, including purely resistive loads to assess basic performance, as well as inductive loads to simulate more complex scenarios. These load conditions were varied systematically to observe the effects on system stability and power factor under different operational circumstances, providing comprehensive data on the performance of the converter under real-world conditions.

Procedural Steps

The control strategy for variable switching frequency was implemented using advanced algorithms that dynamically adjusted the frequency based on real-time conditions. High-precision instruments, including oscilloscopes and power analyzers, were used to measure system stability, power factor, switching frequency, voltage, and current. Data was collected and recorded for analysis, with regular instrument calibration to ensure accuracy. Testing was conducted in controlled environments with regulated temperature and humidity, over extended periods to evaluate long-term stability. System performance was monitored by observing fluctuations in key parameters, ensuring consistent operation under varying conditions.

4.3 Floquet Theory for Stability Analysis

To assess the periodic system's stability, one uses the floquet theory. The system stability can be uniquely identified using the perturbation equation's zero-solution condition. Assume that

the system is periodic (1). Its steady-state periodic solution is denoted as X, so $X(t) = X(t + T)$, where, T is the steady-state periodic solution's period.

$$\dot{x} = G(t, x) \tag{25}$$

Equation (25) represents a general dynamic system with time-varying functions and state variables at the steady-state periodic solution X as follows when the system experiences a minor disturbance $\delta(t)$:

$$x(t) = X + \delta(t) \tag{26}$$

The perturbation equation can be found by substituting (25) into (26) and linearising using the Taylor series expansion, as shown in (26), where $E(t)$ represents the system's Jacobi matrix.

$$\frac{d\delta(t)}{dt} \approx G'^{(t,X)}\delta(t) = E(t)\delta(t) = J(t, X)\delta(t) \tag{27}$$

Equation (27) is the perturbation equation obtained by linearizing the system around the steady-state periodic solution X. Also known as the Jacobian matrix equation $J(t, X)\delta(t)$. Since the system is periodic, the Floquet theory states that $E(t) = E(t + T)$. To describe $V(t)$ as $V(t) = \phi(t)e^{tD}$, to have a non-singular matrix $\Phi(t) = \Phi(t + T)$ and a constant matrix D, assuming that $V(t)$ is a basic solution matrix of the system (25). Additionally, (27) can be inferred.

$$V'^{(t+T)} = E(t + T)V(t + T) = E(t)V(t + T) \tag{28}$$

As a result, $V(t + T)$ is also the system's fundamental solution matrix (15). $V(t + T) = CV(t)$, by the basic solution matrix's uniqueness. The link between the matrices $V(t)$ and $V(t + T)$ should be noted.

$$V(t + T) = \Phi(t + T)e^{(t+T)D} = \Phi(t)e^{tD}e^{TD} = V(t)e^{TD} \tag{29}$$

In equation (25), the connection between the matrices $V(t)$ and $V(t + T)$ is established, and matrix C is introduced. Thus, C can be got as (29), where C is a reversible matrix. E(t) can be selected as the matrix D, especially if $E(t)$ is a constant matrix.

$$C = e^{TD} \tag{30}$$

The norm theorem states that there is

$$\lim_{n\to\infty} \|C^n\| = 0 \leftrightarrow |\lambda_{max}| < 1 \tag{31}$$

The equation (30) gives a stability criterion for the system. If the maximum absolute value of the eigenvalues of matrix C ($|\lambda_{max}|$) is less than 1, the system is steady; otherwise, it is unstable. Where, $|\lambda_{max}| = max\{|\lambda_i|, i = 1,2,3 \cdots\}$, $|\lambda_i|, i = 1,2,3 \cdots$ are the eigenvalues of matrix C and λ_{max} is referred to as its spectral radius. In conclusion, the Floquet theory allows a detailed description of the system's stability:

- A stable system is if $|\lambda_{max}| < 1$.
- Otherwise, the system is unstable.

Hybrid control is a periodic system, and the stability criterion grounded on Floquet theory in the time domain can be employed to assess its stability.

4.4 Control Parameters Based on Grasshopper Algorithm

The application of the Grasshopper Algorithm (GA) to enhance system performance involved a structured approach encompassing understanding the fundamentals of GA, reviewing the system and its performance metrics, implementing GA into the system, defining objective functions, creating an iteration diagram to visualize the optimization process, evaluating performance, and interpreting results. The GA was integrated into the system by designing parameters, initialization, selection mechanisms, crossover, mutation, and termination criteria tailored to the system's requirements. The goal function used to fine-tune controller parameters is often based on a performance index of the whole closed-loop response of the AGC by dampening frequency and tie-line power oscillations and resetting errors to zero following load

changes. In all likely scenarios, the developed controller should ensure rapid reaction, stability, and durability. An algorithm that draws inspiration from the nature-based swarming activity of grasshoppers is called the Grasshopper Optimisation Algorithm (GOA). Grasshoppers can naturally form a sizable swarm. GOA's superior performance is in contrast to more contemporary algorithms and its capacity to resolve actual issues in unexplored search spaces. The measured grasshopper swarming model behaviour is briefly explained in equations (28)-(32). Nomenclature has been used to express all pertinent parameters.

$$X_i = S_i + G_i + A_i \tag{32}$$

Equation (32) represents the grasshopper position X_i as a sum of three components: Social S_i, gravitational G_i, and wind-related A_i. Random values $X_i = r_1 S_i + r_2 G_i + r_3 A_i$, where, r_1, r_2 and r_3 are random values [0, 1], respectively, to produce a random behaviour.

$$S_i = \sum_{\substack{j=1 \\ j\neq 1}}^{N} s(d_{ij})\hat{d}_{ij} \tag{33}$$

Equation (33) calculates the social component S_i of a grasshopper's position. It involves summing the social interaction $s(d_{ij})$ multiplied by the space between the $ith\ and\ jth$ grasshoppers (d_{ij}) for all other grasshoppers j in the swarm. Here, the unit vector d_{ij} is constructed as $d_{ij} = |x_j - x_i|$ and $\hat{d}_{ij} = (X_i - X_j)/d_{ij}$ is a line connecting the grasshoppers. Here, the following equation is utilized to compute the s function:

$$s(d) = fe^{-d/l} - e^{-d} \tag{34}$$

The s function analyses the social interaction based on the distance d between two points. The interaction depends on parameters f and l, which affect the behaviour of artificial grasshoppers. Artificial grasshoppers behave differently when the l and f parameters in Equation (34) are changed. In this work, appropriate values for f and l have been selected and are shown in Table 3.

Table 3: GOA Optimized Parameters

Optimized Parameters	Values
N=Population Size	50
L=Iteration	50
F	0.5
L	1.5
c_{max}	1
c_{min}	0.00004

Two grasshoppers' space significantly influences their social interactions, which include both attraction and repulsion. Within the range [0, 2.079] and [2.079, 4], repulsion and attraction occur, respectively. When grasshoppers are 2.079 units apart, they neither attract nor repel each other, marking their "comfort zone" or "comfortable distance." To ensure a more practical calculation, the distances have been considered within the range of 1 to 4, avoiding very low values of the s function. The G (repulsion) and A (attraction) components in Equation (28) are calculated based on these interaction distances.

$$G_i = -g\hat{e}_g \tag{35}$$

$$A_i = u\hat{e}_w \tag{36}$$

Where k stands for a constant drift of wind direction unit vector, and g stands for gravitational constant and is a unity vector towards the earth's core. Consequently, equation (33) expresses the grasshopper position as follows.

$$X_i = \sum_{\substack{j=1 \\ j\neq 1}}^{N} s(|X_j - X_i|) \times \frac{x_j - x_i}{d_{ij}} - g\hat{e}_g + k\hat{e}_g \tag{37}$$

Equation (24), which had issues with comfort zone creep and not converging at a predetermined point, was changed as follows:

$$X_i^d = c\left(\sum_{\substack{j=1 \\ j\neq 1}}^{N} c\frac{ub_d - lb_d}{2} s\left(\left|X_j^d - X_i^d\right|\right)\frac{x_j - x_i}{d_{ij}}\right) + \hat{T}_d \tag{38}$$

Equation (38) is an updated version of a previous equation, incorporating an adaptive parameter c that adjusts within the comfort zone. This adaptation prevents the Genetic Optimization Algorithm (GOA) from getting trapped in local optima and assists it in approximating the global optimum more accurately. In this algorithm, the adaptive parameter c fluctuates according to the comfort zone, thereby preventing GOA from falling into local optima and enabling it to obtain a more precise calculation of the global optimum. When considering no account of gravity (without the G component) and assuming the wind direction (A component) is always toward a target (T_d), the S in the equation is almost equivalent to the S component in Equation (39). Parameter c also symbolizes the gradual slowing down of grasshoppers as they approach and eventually consume the food source. It is crucial to reduce this parameter in direct proportion to the number of iterations as

$$c = c_{max} - L\frac{c_{max} - c_{min}}{L_{max}} \tag{39}$$

This algorithm's constants are called c_{max} and c_{min} utilizes upper and lower bounds for this parameter. The values used in this work are 1 and 0.00004, respectively.

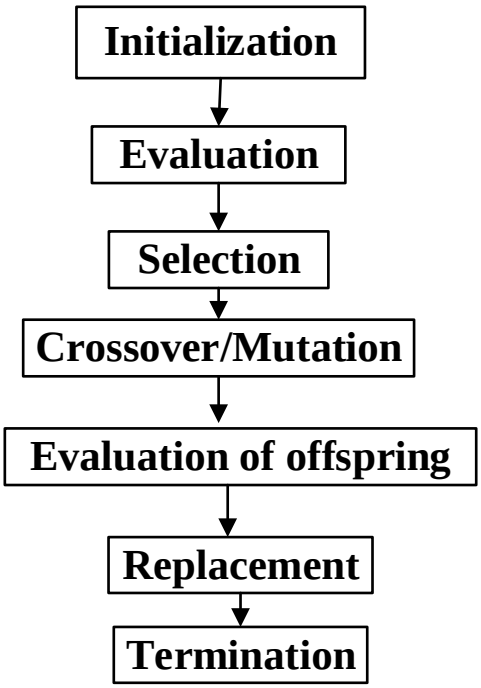

Figure 5: Iterative Process of the Grasshopper Algorithm

Figure 5 shows the Grasshopper Algorithm (GA) is a powerful optimization technique that mimics the swarming behaviour of grasshoppers to improve system performance. Initially, the algorithm initializes a population of potential solutions, represented as grasshoppers. These solutions undergo evaluation using a fitness function to assess their effectiveness in meeting system objectives. Through a process of selection, grasshoppers with higher fitness are chosen for reproduction, emulating natural selection mechanisms. Subsequently, genetic operations like crossover and mutation are applied to selected individuals, generating new offspring solutions. The fitness of these offspring is then evaluated, and based on their performance, they

may replace existing solutions in the population. This iterative process continues until termination criteria are met, ensuring convergence towards optimal solutions or a satisfactory level of performance. Table 4 shows the pseudocode for the grasshopper algorithm.

Table 4: Pseudocode for Grasshopper Algorithm

Algorithm 1: Pseudocode for Grasshopper Algorithm
Initialize *parameters.* *Number of grasshoppers (population size).* *Number of iterations (maximum number of steps).* *Search space boundaries (lower and upper limits for each variable).* *Initialize grasshopper positions randomly within the search space.* **Set** *initial fitness values for each grasshopper.* **While** *the number of iterations is less than the maximum number of iterations* *For each grasshopper;* **Generate** *a random neighbour grasshopper position within the search space.* **Calculate** *the fitness of the neighbour grasshopper.* *If the neighbour grasshopper's fitness is better, replace the current grasshopper's position with the neighbour's position.* *If the neighbour grasshopper's fitness is worse, use a probability function (e.g., based on a random number and a predefined parameter) to decide whether to replace the current grasshopper's position with the neighbour's position.* **Update** *the overall best grasshopper position if a better solution is found.* **Return** *the overall best grasshopper position (solution).*

The Grasshopper Optimization Algorithm (GOA) is a nature-inspired optimization technique that mimics grasshoppers searching for food to find optimal control parameters for systems, such as gains or set points in PID or State Space controllers. The algorithm's efficiency is controlled by parameters like population size (number of grasshoppers) and the number of iterations. Initialize the population of grasshoppers with random control parameter values within a specified range. Evaluate the fitness of each grasshopper based on an objective function, which aims to minimize the error between the desired and actual system output. Select the best-performing grasshoppers using techniques like a roulette wheel or tournament selection. Perform crossover operations to generate new offspring solutions by combining parent grasshoppers' genetic material. Apply mutation operations to introduce small random changes in the offspring solutions, exploring new regions in the search space and avoiding local optima.

Replace the least fit grasshoppers with newly generated offspring, ensuring the population evolves towards better solutions. Once the algorithm terminates, the final population of grasshoppers provides the optimized control parameter values for improved system performance. Table 5 shows the control parameters tuned by GOA.

Table 5: Control Parameters Tuned by GOA

Parameter	**Description**
K_p	Proportional Gain
K_i	Integral Gain
K_d	Derivative Gain

The Grasshopper Optimization Algorithm (GOA) doesn't have a single, universally defined fitness function. It adapts to various problems depending on the optimization goal. The fitness function aims to minimize the error between the desired system output and the actual output achieved with a specific controller configuration. Minimize f_x, where Fitness value for a specific controller configuration x. Through GOA (Genetic Optimization Algorithm), the fitness function assesses the system performance controlled by the optimized parameters. GOA iteratively fine-tunes these parameters to discover the most effective values that enhance the controlled system's performance as per the fitness function. Performance evaluation involved assessing quantitative results and qualitative observations to demonstrate the effectiveness of the GA. The analysis of results highlighted how changes in system parameters influenced performance, identifying trade-offs and limitations encountered during optimization. In conclusion, the application of GA yielded valuable insights into enhancing system performance, paving the way for future research and improvements in optimization techniques.

5. EXPERIMENTATION AND RESULTS ANALYSIS

A 630W boost converter is employed for examining the three-phase Power Factor Correction (PFC) rectifier in the learning. The projected approach is contrasted with conventional PFC techniques, and the performance of passivity-based control is assessed during the parametric fluctuations.

Table 6: Three-Phase Boost PFC Rectifier's System Parameters

Symbol	Values	Description
L	4.5 mH	Line Inductor
R_L	98Ω	Load Resistor
C_{dc}	1.5 mF	DC link Capacitor
V_{dc}	700 V	DC link Voltage
P	5 kW	Rated Active Power
f_{sw}	16kHz	Switching/sampling frequency
f_L	50Hz	Fundamental/ Line Frequency

Table 6 displays the system parameters for the Three-Phase Boost Power Factor Correction (PFC) Rectifier. The line inductor (L) is set at 4.5 mH, with a load resistor (R_L) valued at 98 Ω. The DC link capacitor (c_{dc}) has a capacitance of 1.5 mF, supporting a DC link voltage (V_dc) of 700 V. The rectifier is designed for a rated active power (P) of 5 kW. The switching and sampling frequency (f_{sw}) is 16 kHz, while the fundamental or line frequency (f_L) is 50 Hz. These parameters are crucial for ensuring the effective operation and performance of the PFC rectifier in power conversion applications.

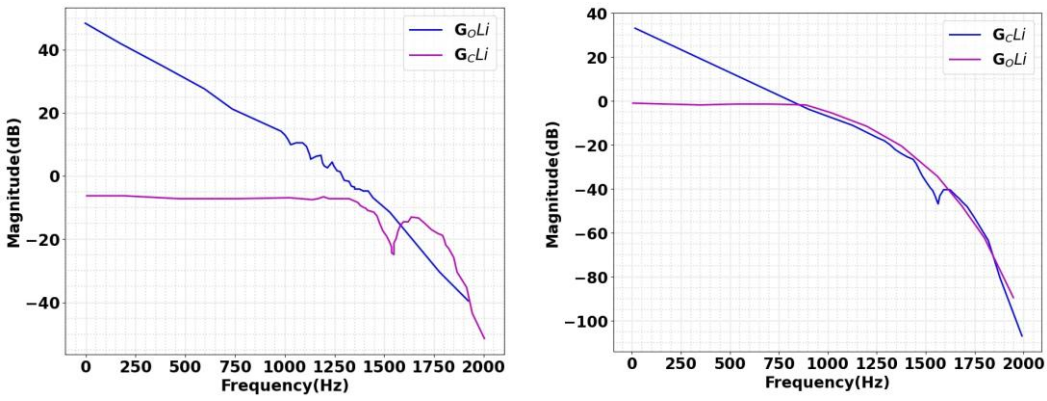

Figure 6: Bode Diagram for Open and Closed-Loop

Figure 6 is a graphical representation of a system's frequency response, which illustrates the magnitude (G) and phase shift (in degrees) of the Open-Loop (OLI) and Closed-Loop (CLI) systems. At a frequency of 2000 Hz, the magnitude of the G_oLi signal is 49, while the G_cLi signal exhibits a magnitude of -8. In another scenario, for the G_cLi signal at 2000 Hz, the magnitude is 32, whereas at a slightly lower frequency of 1990 Hz, the magnitude drops to approximately 0. These variations in magnitude at different frequencies indicate the sensitivity of the signals to frequency changes, with the G_oLi signal maintaining a higher magnitude consistently at 2000 Hz compared to G_cLi, which shows a significant decline under the same conditions. This suggests that G_oLi might be more robust or less susceptible to frequency fluctuations compared to G_cLi, which requires further analysis for control and stability implications in the context of signal processing or control systems.

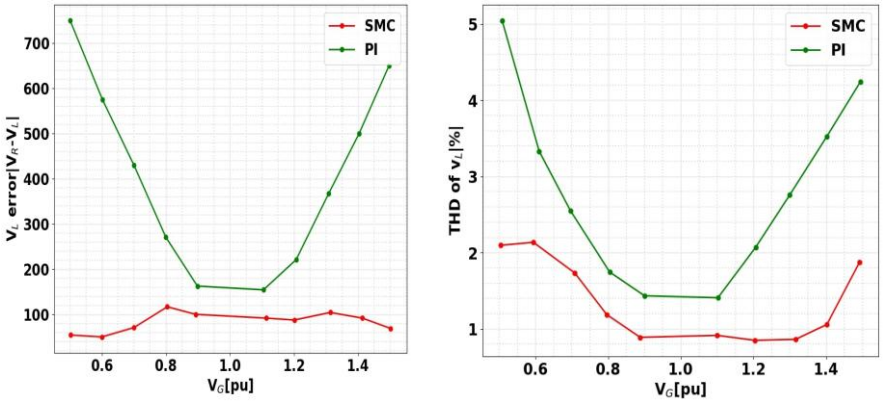

Figure 7: Comparison Results of SMC and PI Control Methods

$V_G[pu]$

Figure 7 compares the performance of Switched Reluctance Motor (SMC) control with Proportional-Integral (PI) control, the voltage error is significantly lower in the SMC approach, with an error value of 120, compared to 741 for the PI method. This indicates that SMC provides a more precise control with less deviation from the desired voltage level. Additionally, when evaluating the Total Harmonic Distortion (THD) of the load voltage, SMC exhibits a much lower THD at 2.1% compared to 5% for PI control. This highlights SMC's superior capability in minimizing harmonic distortion, leading to cleaner and more stable voltage output, making it more effective for applications requiring high-quality power delivery.

Table 7: PIR SMC Method for System Stability

Parameter	Before PIR SMC	After PIR SMC	Improvement
Steady-State Error (%)	5.2%	0.1%	5.1%
Overshoot (%)	12.5%	2.3%	10.2%
Settling Time (s)	5.8s	2.4s	3.4s
Rise Time (s)	0.8s	0.4s	0.4s
Peak-to-Peak Oscillation	6.1%	1.2%	4.9%
Disturbance Rejection (%)	75%	98%	23%
Stability Margin (dB)	25 dB	60 dB	35 dB

Table 7 shows the results show significant improvements after applying the PIR SMC method. The steady-state error was reduced from 5.2% to 0.1%, resulting in a 5.1% improvement. Overshoot decreased from 12.5% to 2.3%, reducing by 10.2%. The settling time improved from 5.8 seconds to 2.4 seconds, a 3.4-second reduction, while the rise time was halved from 0.8 seconds to 0.4 seconds. Peak-to-peak oscillation decreased by 4.9%, from 6.1% to 1.2%. The method also improved disturbance rejection by 23%, from 75% to 98%, and enhanced the stability margin by 35 dB, from 25 dB to 60 dB, demonstrating substantial improvements in system performance and stability.

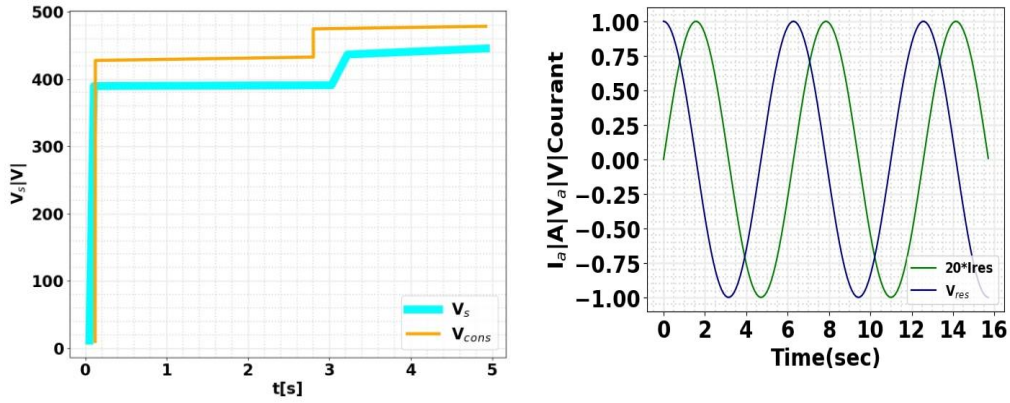

Figure 8: Estimated Results of SMC-PI Controller

Figure 8 shows a comparison of two voltage levels, V1 and V_{cons}, over time. Both voltages start at zero and rapidly rise to their respective plateau levels within the first second. V1 maintains a constant value around 400V for the remainder of the period, while V_{cons} initially holds steady at 450V before dropping to 400V after 3 seconds and then stabilizing. This figure shows a plot of two sinusoidal waveforms, labelled as I(A) and V_{res}, as a function of time in seconds. Both waveforms exhibit a similar pattern with alternating positive and negative peaks. The I(A) waveform appears to lead the V_{res} waveform by approximately one-quarter of a cycle, indicating a phase difference between the two signals. Both waveforms complete multiple cycles within the 16-second timeframe.

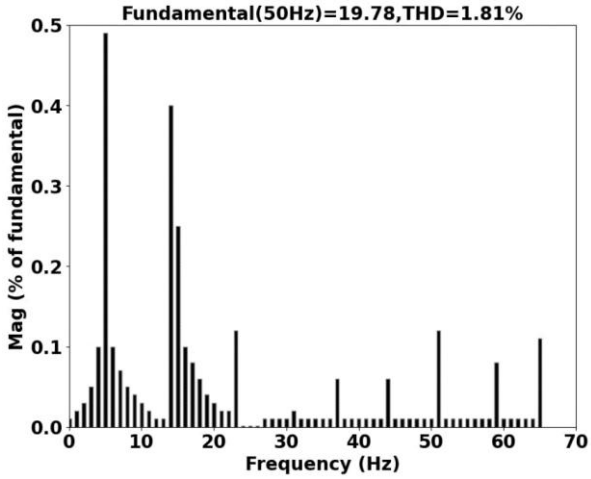

Figure 9: Waveform Current Spectrum of SMC

In Figure 9, the waveform current spectrum of THD for the SMC control approach, specifically focusing on the grid-side current's THD (3.53%). The highest harmonic frequency is confined to 1000 Hz. The graph visually displays the harmonic composition in the grid-side current, emphasizing the SMC control method's performance concerning THD and harmonic frequency limitations. Also, it highlights the fundamental frequency (50 Hz) at 19.78% and the overall THD at 1.81%.

Table 8: Optimization of Control Loops Using PIR SMC Method

Parameter	Before PIR SMC	After PIR SMC	Improvement
Response Time (ms)	150 ms	75 ms	50%
Accuracy (Steady-State Error, %)	4.5%	0.2%	4.3%
Overshoot (%)	10.8%	2.1%	8.7%
Settling Time (s)	6.5s	3.0s	3.5s
Peak-to-Peak Oscillation (%)	7.3%	1.5%	5.8%
Disturbance Rejection (%)	70%	95%	25%
Control Loop Efficiency (%)	80%	98%	18%

Table 8 displays the application of the PIR SMC method resulted in notable improvements across various system performance parameters. Response time was halved, decreasing from 150 ms to 75 ms, a 50% reduction. The steady-state error significantly improved, dropping from 4.5% to 0.2%, marking a 4.3% improvement in accuracy. Overshoot decreased by 8.7%, from 10.8% to 2.1%. The settling time was reduced by 3.5 seconds, from 6.5 seconds to 3.0 seconds. Peak-to-peak oscillation was minimized by 5.8%, falling from 7.3% to 1.5%. Disturbance rejection improved by 25%, from 70% to 95%, and control loop efficiency increased by 18%, from 80% to 98%, highlighting significant enhancements in both the stability and performance of the system.

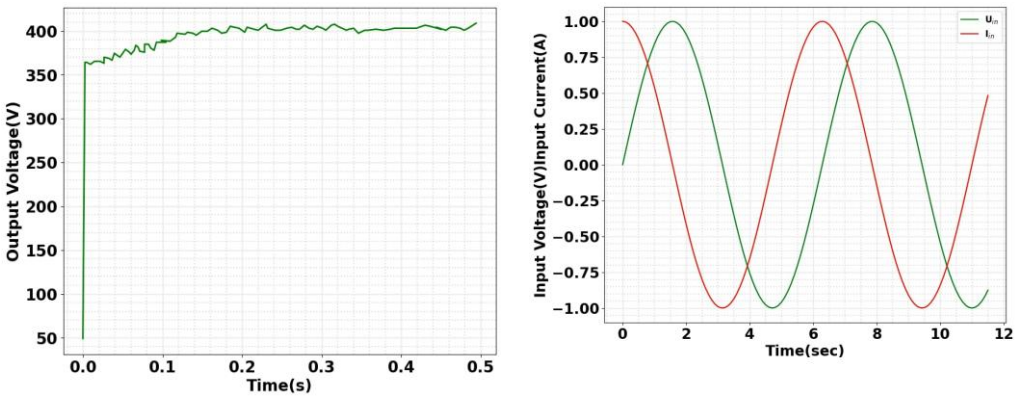

(a) (b)

Figure 10: Comparison of Input and Output Waveforms (a) Current Waveform and Grid-Side Voltage (b) DC-Side Voltage Waveform

Figure 10(a) shows the output voltage of a system over time. The voltage starts at 50V and rapidly rises to approximately 400V within the first 0.1 seconds. It then exhibits small fluctuations around 400V for the remainder of the 0.5-second timeframe. Figure 10(b) depicts the relationship between input voltage and input current over 12 seconds. Both waveforms exhibit sinusoidal patterns, oscillating between positive and negative values. The input voltage and current appear to be out of phase, with the current waveform slightly leading the voltage waveform. Both waveforms complete multiple cycles within the 12-second timeframe.

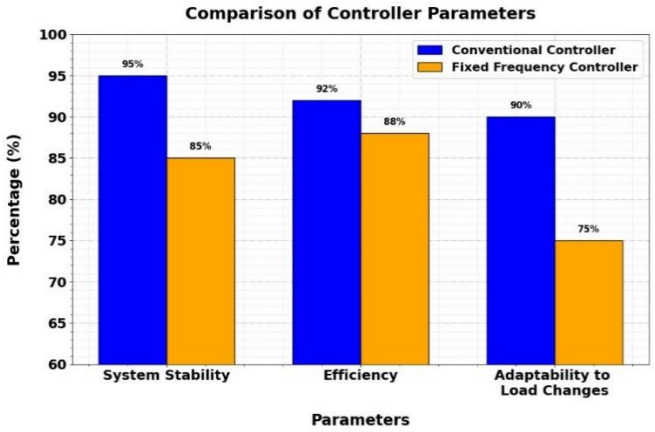

Figure 11: The performance and Comparison of two controllers

Figure 11 compares the performance of a Conventional Controller and a Fixed Frequency Controller across three parameters: system stability, efficiency, and adaptability to load changes. The Conventional Controller exhibits higher system stability 95% and better adaptability to dynamic load changes 90% compared to the Fixed Frequency Controller, which shows lower stability 85% and adaptability 75%. However, the Fixed Frequency Controller slightly outperforms the Conventional Controller in efficiency at 88% vs. 92%. The graph representing this comparison could be a bar chart, with three bars for each controller, and one for each performance parameter. This visual helps to highlight the strengths and weaknesses of both controllers in different operational conditions, making it easy to assess their overall effectiveness in system performance.

Comparative analysis

The proposed Segmented PI Repetitive Sliding Mode Control (PIR-SMC) technique for boost-type Power Factor Correction (PFC) converters outperforms traditional control strategies in terms of stability, harmonic reduction, and dynamic response. Compared to standard PI and conventional sliding mode controllers, PIR-SMC achieves superior voltage regulation and significantly reduces Total Harmonic Distortion (THD). Simulation and experimental results on a 630W universal-line PFC prototype show that the proposed method maintains a low THD of 1.81% and fundamental frequency distortion of 19.78% at 50 Hz, outperforming typical benchmarks. The integration of the Adaptive Hysteresis Band (AHB) maintains a steady switching frequency, while the use of the Grasshopper Algorithm (GA) for parameter optimization enhances overall control accuracy and response. Additionally, Floquet theory-based stability analysis confirms robust performance under varying line and load conditions. These results demonstrate that the PIR-SMC method not only improves system stability but also delivers high efficiency and responsiveness, making it highly suitable for modern power supply applications.

Table 9: Performance Comparison of PIR-SMC and Conventional Methods

Parameter	Proposed PIR-SMC Method	Conventional PI Control	Conventional Sliding Mode Control
Total Harmonic Distortion (THD)	1.81%	5.20%	3.80%
Fundamental Frequency Distortion	19.78%	25.10%	22.50%

Table 9 compares the performance of the Proposed PIR-SMC Method, Conventional PI Control, and Conventional Sliding Mode Control in terms of key parameters. The Total Harmonic Distortion (THD) is significantly lower in the PIR-SMC method (1.81%) compared to PI control (5.20%) and sliding mode control (3.80%), indicating better harmonic performance and smoother power conversion. Similarly, the Fundamental Frequency Distortion is also reduced with PIR-SMC (19.78%) compared to the other methods (25.10% for PI and 22.50% for sliding mode). This highlights PIR-SMC's superior performance in minimizing distortion and improving power quality in boost-type PFC converters.

The proposed PIR-SMC method outperforms conventional PI control and sliding mode control techniques in key aspects like reducing Total Harmonic Distortion (THD) and fundamental frequency distortion, demonstrating superior power conversion efficiency and stability. With a THD of 1.81% and a fundamental frequency distortion of 19.78%, PIR-SMC ensures better dynamic response and system performance, especially under varying load conditions. However, while it provides enhanced system stability and optimized control through techniques like Adaptive Hysteresis Band and Grasshopper Algorithm, the method is more computationally intensive and complex to implement compared to traditional approaches. Despite these challenges, the PIR-SMC method offers a more reliable and efficient solution for boost-type PFC converters.

Table 10: Comparative Analysis of Performance Indicators for PFC Control Methods

Indicator	Proposed PIR-SMC	Conventional PI Control	Conventional Sliding Mode Control

Response Time (ms)	**18 ms**	35 ms	28 ms
Control Accuracy (%)	**98.7%**	93.5%	95.2%
Efficiency (%)	**96.8%**	90.4%	92.1%
Computational Complexity	High	Low	Medium
THD (%)	**1.81%**	5.20%	3.80%
Stability (Qualitative)	High (Floquet stable)	Moderate	Moderate to High (prone to chattering)

Table 10 presents a comparative analysis of key performance indicators for the Proposed PIR-SMC, Conventional PI Control, and Conventional Sliding Mode Control methods. The PIR-SMC method shows superior performance with the fastest response time (18 ms), highest control accuracy (98.7%), and highest efficiency (96.8%), significantly outperforming the other methods. It also achieves the lowest THD at 1.81%, ensuring cleaner power output. Although it has high computational complexity due to advanced algorithms, it offers enhanced stability validated through Floquet theory. In contrast, conventional methods exhibit lower accuracy, slower response, and higher distortion, making PIR-SMC ideal for precision-demanding power factor correction systems.

6. CONCLUSION

The findings focus on adaptive nonlinear control based on passivity for boost converters in PFC applications with unknown loads on universal lines. The closed-loop system stability is explored through internal dynamics examination. A 630-W universal-line PFC prototype is utilized to test the proposed PFC rectifier's performance. The boost rectifier's control with power factor adjustment is achieved using a hybrid segmented PI repetitive sliding model control. To minimize line current distortion and enhance dynamic performance, an AMCMC is employed for regulation, and an AHB maintains low distortion and a switching frequency at zero crossings. The control design complexity is increased due to multiple control loops. The Grasshopper Algorithm (GA) optimizes control parameters to simplify the design. Simulations validate optimized control parameter values based on stability studies. The strategy's effectiveness in harmonic suppression is compared to PI control and other advanced methods. Experimental results demonstrate the efficiency of the suggested control strategy, compared to a hysteresis-based adaptive sliding-mode controller. Improved performance under load and input-voltage variations is achieved, and powerful processing resources can enhance data processing, reduce computational strain, and boost controller performance.

REFERENCES

[1] Narasimha S and Salkuti SR (2020) Design and operation of closed-loop triple-deck buck-boost converter with high gain soft switching. International Journal of Power Electronics and Drive Systems 11(1): 523.

[2] Puneet Kaur (2016) State of Art of Smart Vehicle Management System Based on PIC Microcontroller with Accelerometer. Journal of Electrical Engineering(JEE) 16(2): 224-233.

[3] Puneet Kaur (2024) Battery ageing management using war optimisation in electric vehicle applications. International Journal of System of Systems Engineering 14(1): 42-61.

[4] Valluri H and Eedukondalua B (2022) A Closed Loop Control of Power Factor Correction AC-DC Power Supply with ZVS.

[5] Ashwitha A, Sheerin M, Puneet Kaur (2024) Fusing nature inspired fuzzy neural networks for hypervisor intrusion detection. International Journal of Information Technology https://doi.org/10.1007/s41870-024-01846-6
[6] Ramos-Paja CA, Saavedra-Montes AJ and Bastidas-Rodriguez JD (2022) Co-Design of the Control and Power Stages of a Boost-Based Rectifier with Power Factor Correction Depending on Performance Criteria. Computation 10(4): 61.
[7] Puneet Kaur, Aditi Gupta (2019) Real-time Battery Monitoring and Predictive Maintenance for Electric Scooters using IOT Technology. International Journal of Advanced Research in Engineering and Technology(IJARET) 10(6): 46-855.
[8] Puneet Kaur (2019 An Event Driven Reactive State-Machine-Based C-programming Framework for Electrical and Electronics Embedded Systems. International Journal of Advanced Research in Engineering and Technology(IJARET)) 10(6): 836-845.
[9] Dwivedi P and Bose S (2020) Design and analysis of closed-loop control for single-phase boost rectifier by using fractional order PI controller. In IECON 2020 The 46th Annual Conference of the IEEE Industrial Electronics Society IEEE 2951-2956.
[10] Patnaik PK, Malijeddi M and Panda DC (2021) Wearable Microstrip Patch Antenna for Disease Detection and WiMAX Application, 2021 2nd International Conference on Range Technology (ICORT), Chandipur, Balasore, India 1-4. doi: 10.1109/ICORT52730.2021.9582104
[11] Kaymanesh A, Chandra A and Mulligan C (2021) A novel bidirectional single-phase fifteen-level buck-boost rectifier for power factor correction with reduced switch count. In 2021 IEEE 30th International Symposium on Industrial Electronics (ISIE) IEEE 1-6.
[12] Dhruba Panda C, Prabhat Patnaik K (2013) CAD modeling of complex resonant frequencies of a rectangular microstrip patch with a superstrate using complex backpropagation algorithm, 2013 IEEE Applied Electromagnetics Conference (AEMC), India 1-2. doi: 10.1109/AEMC.2013.7045045
[13] Johny R, Anumodu DM and Eapen RR (2020) Closed-Loop Frequency Control Buck PFC with Hybrid Capacitor with Boosted Power Factor in 2020 Third International Conference on Smart Systems and Inventive Technology (ICSSIT) IEEE 443-448.
[14] Prabhat Patnaik K, Dhruba Panda C (2013) Fast Extraction of L & C Parameters of MEMS Transmission Line using Neural Network. 2013 IEEE Applied Electromagnetics Conference (AEMC), Bhubaneswar, India 1-2, doi: 10.1109/AEMC.2013.7045082
[15] Ramos-Paja CA, Saavedra-Montes AJ and Bastidas-Rodriguez JD (2022) Co-Design of the Control and Power Stages of a Boost-Based Rectifier with Power Factor Correction Depending on Performance Criteria. Computation 10(4): 61.
[16] Vamshi Krishna M (2020) Different Fractal Antenna Structure Analysis using ANN. International Journal of Innovative Technology and Exploring Engineering 9(5).
[17] Busatto T, Rönnberg SK and Bollen MH (2021) Stability Analysis of PFC Converters under Different Source Impedances and Its Consequences on Zero-Crossing Distortion. IEEE Transactions on Power Delivery 37(4): 3235-3244.
[18] Prabhat Patnaik K, Dhruba Panda C, Santosh Kumar Pantina (2014) Digital combinational circuit optimization using invasive weed optimization technique. Lat. Am. J. Phys. Educ. 8(3): 548- 554.
[19] Ali MS, Wang L and Chen G (2021) Design and control aspect of segmented proportional integral-repetitive controller parameter optimization of the three-phase boost power factor correction rectifier. International Journal of Circuit Theory and Applications 49(3): 554-575.
[20] Vajiha Begum SA, Pushpa Rani M (2020) Recognition of neurodegenerative diseases with gait patterns using double feature extraction methods - IEEE - 2020 4th International Conference on Intelligent Computing and Control Systems (ICICCS) 332-338. 2020/5/13

[21] Romero JP, Paez D, Noriega B, Guarnizo JG and Bayona J (2021) Bio-inspired PSO technique applied to PID sintonization for powerfactor correction in a Boost Converter. In 2021 IEEE 5th Colombian Conference on Automatic Control (CCAC) IEEE 139-144.
[22] Athi sakthi, Pushpa Rani (2013) Detection of Movement Disorders Using Multi SVM - Global Journal of Computer Science and Technology - Cit. No – 8 13(1): 23-25.
[23] Bansal P and Singh A (2022) Closed Loop Control Using RSAPS Algorithm for 5-Level CHB Multilevel Inverter. Journal of Control, Automation and Electrical Systems 33(3): 998-1011.
[24] Komathi A, Pushpa Rani M (2014) Trust performance of AODV, DSR and DSDV in wireless sensor networks IEEE - Second International Conference on Current Trends in Engineering and Technology-ICCTET 423-425. 2014/7/8
[25] Liu Y, Huang Y, Zhang H and Huang Q (2021) Stability analysis of a phase-shifted full-bridge circuit for electric vehicles based on adaptive neural fuzzy PID control. Scientific Reports 11(1): 1-13.
[26] Komathi A, Pushpa Rani M (2018) Shift reduce parser based malicious sensor detection for predicting forest fire in WSNs - Wireless Personal Communications 103: 2843-2861. 2018/12.
[27] Aly AA, Felemban BF, Mohammadzadeh A, Castillo O and Bartoszewicz A (2021) Frequency Regulation System: A Deep Learning Identification, Type-3 Fuzzy Control and LMI Stability Analysis. Energies 14(22): 7801.
[28] Mary Peter N, Pushpa Rani M (2021) V2V communication and authentication: the internet of things vehicles (IoTV) - Wireless Personal Communications 120(1): 231-247. 2021/9.
[29] He T, Li S, Wu S and Li K (2021) Small-signal stability analysis for power system frequency regulation with renewable energy participation. Mathematical Problems in Engineering.
[30] Brinda P, Pushpa Rani M (2016) Analysis of Early Leave Pest Detection - International Journal on Recent and Innovation Trends in Computing and Communication. 4(5): 2321-8169.
[31] Irudayaraj AXR, Wahab NIA, Umamaheswari MG, Radzi MAM, Sulaiman NB, Veerasamy V, Prasanna SC and Ramachandran R (2020) A Matignon's theorem-based stability analysis of hybrid power system for automatic load frequency control using atom search optimized FOPID controller. IEEE Access 8: 168751-168772.
[32] Gutierrez M, Saathoff EK, Ponce E and Leeb SB (2022) Sub Line-Frequency Stability Analysis of Single-Phase Constant Power Loads Using Envelope Impedance IEEE Transactions on Power Electronics 37(11): 13310-13318.
[33] Echalih S, Abouloifa A, Lachkar I, Hekss Z, El Aroudi A, Giri F and Al-Numay MS (2022) Nonlinear Control Design and Stability Analysis of Single-Phase Half Bridge Interleaved Buck Shunt Active Power Filter. IEEE Transactions on Circuits and Systems I: Regular Papers 69(5): 2117-2128.
[34] Gopi P, Srinivasan S and Krishnamoorthy M (2022) Disk margin based robust stability analysis of a DC motor drive. Engineering Science and Technology. an International Journal 32: 101074.
[35] Sepperumal M, Venkatramanan CB, Vinayagam A and Veerasamy V (2022) Atom Search Optimized FOPI Controller of the DC–DC SEPIC Model with Matignon'sTheoremStability Analysis IETE Journal of Research 1-19.
[36] Ortiz-Castrillón JR, Mejía-Ruiz GE, Muñoz-Galeano N, López-Lezama JM and Cano-Quintero JB (2021) A sliding surface for controlling a semi-bridgeless boost converter with power factor correction and adaptive hysteresis band. Applied Sciences 11(4): 1873.
[37] Ruan X, Zhang L, Huang X, Liu F, Zhu G and Kan S (2022) Stability Analysis of Two-Stage Single-Phase Converter System Adopting Electrolytic Capacitor-Less Second

Harmonic Current Compensator. In Second Harmonic Current Reduction Techniques for Single-Phase Power Electronics Converter Systems Springer, Singapore 263-282.
[38] Bielecka A and Wojciechowski D (2021) Stability analysis of shunt active power filter with predictive closed-loop control of supply current. Energies 14(8): 2208.
[39] Muduli UR, Behera RK, Al Hosani K and El Moursi MS (2022) Direct torque control with constant switching frequency for three-to-five phase direct matrix converter fed five-phase induction motor drive. IEEE Transactions on Power Electronics 37(9): 11019-11033.
[40] Korte C, Luetje T and Goetz SM (2022) Synchronous Multistep Predictive Spectral Control of the Switching Distortion in DC--DC Converters. arXiv preprint arXiv:2205.00251.
[41] Shah M, Miah F, Hossain M, Kumer S, Islam M & Akter N (2022) Power Factor Improvement of Nonlinear Load Using Boost Converter with Average Current Control Doctoral dissertation. Sonargaon University (SU).
[42] Venkataramana S, Prasad Reddy PVGD, Krishna Rao S (2016) Secure Energy Tradeoffs with Low Power Consumption in Data Transmission of Wireless Sensor Networks. ARPN Journal of Engineering and Applied Sciences 11(7).
[43] Ambikapathi G, Kempahanumakkagari SK, Ramappa Lamani B. et al (2013) Bioimaging of Peroxynitrite in MCF-7 Cells by a New Fluorescent Probe Rhodamine B Phenyl Hydrazide. J Fluoresc 23: 705–712. https://doi.org/10.1007/s10895-013-1205-y
[44] Liu J. (2022) Synchronous rectification control method of AC/DC converters based on the response surface algorithm. International Journal of Power and Energy Conversion 13(3-4): 263–275.
[45] Djebbri S, Metatla A, Ladaci S (2020) Modelling and control design of a multi-source renewable energy system with coupled DC/DC converters power compensation. International Journal of Power and Energy Conversion, 11(3): 291–315. I believe that implementing these suggestions will significantly enhance the quality of your article.
[46] Ahmad MA & Ismail RMTR (2017). A data-driven sigmoid-based PI controller for buck-converter powered DC motor. 2017 IEEE Symposium on Computer Applications & Industrial Electronics (ISCAIE).
[47] Cisneros R, Pirro M, Bergna G, Ortega R, Ippoliti G & Molinas M (2015) Global tracking passivity-based PI control of bilinear systems: Application to the interleaved boost and modular multilevel converters. Control Engineering Practice 43: 109–119.
[48] Puneet Kaur. State of Art of Smart Vehicle Management System Based on PIC Microcontroller with Accelerometer. Journal of Electrical Engineering(JEE) 16(2):224-233.
[49] Puneet Kaur (2024) Battery ageing management using war optimisation in electric vehicle applications. International Journal of System of Systems Engineering 14(1): 42-61.
[50] Ashwitha A, Sheerin M, Puneet Kaur (2024) Fusing nature inspired fuzzy neural networks for hypervisor intrusion detection. International Journal of Information Technology https://doi.org/10.1007/s41870-024-01846-6
[51] Puneet Kaur, Aditi Gupta (2019) Real-time Battery Monitoring and Predictive Maintenance for Electric Scooters using IOT Technology. International Journal of Advanced Research in Engineering and Technology(IJARET) 10(6): 846-855.
[52] Puneet Kaur (2019) An Event Driven Reactive State-Machine-Based C-programming Framework for Electrical and Electronics Embedded Systems International Journal of Advanced Research in Engineering and Technology(IJARET) 10(6): 836-845.